ENCODING PROTEST DURATION IN AN AGENT-BASED MODEL AS CHARACTERISTIC PHASE TRANSITIONS

Brian J. Goode
Bianica Pires

The MITRE Corporation
7596 Colshire Drive
McLean, VA, USA
{bgoode, bpires}@mitre.org

ABSTRACT

Protests and civil unrest events carry high societal impact and are examples of complex interactions and collective behavior. Agent-based modeling (ABM) is one approach to simulating emergent phenomena seen in protests by leveraging individual behaviors derived from theory or observation. The utility of these models is immense; however, techniques for understanding the theoretical consonance of these complex aggregate behaviors is missing. For example, protest dynamics can range from small-scale, more frequent protests to nation-wide events that can last several days. This work focuses on characterizing the duration between population level shifts from protest and non-protest states using a characteristic, stylized, network model of individual interactions. The model encodes the population (macro-)level protest states as a well-known phase transition (double-well potential function) dependent on individual (micro-)level interaction characteristics. The model is fit to the ABM in distribution and the process of rioting is captured by a reduced set of parameters.

Keywords: protests, agent-based modeling, model reduction, model characterization.

1 INTRODUCTION

Protests are examples of collective behavior in a population bringing widespread attention to particular causes or issues (Casper and Tyson 2014, Fowler and Christakis 2010, González-Bailón et al. 2011). It is one example of dynamics that are described by complex, multi-scale processes (e.g., West and Grigolini 2011) having similarities to weather (Lorenz 1963), financial (Mandelbrot and Hudson 2006), and neuro-physiological modeling (Nicolelis 2012). Individual interactions on a micro-level result in observed macro-level effects or phase transitions. From a network structure perspective, one potential source of complexity in protest formation is the impact on spreading phenomena by the structure of social networks (Pires and Crooks 2017).

The interplay between individual dynamics and population-level observables is seen in a number of ways. Spatial effects over social networks on global civil unrest are explicitly discussed by (Braha 2012). Clauset, Young, and Gleditsch (2007) analyze the occurrence rate of severe terrorist events through the lens of a power law distribution. Similarly, Johnson et al. (2013) show how the timing of human confrontations, including civil-unrest, follow a power law distribution.

Approved for Public Release; Distribution Unlimited. Public Release Case Number 22-0706.

Capturing these dynamics in a model that is useful, replicable, and reproducible is not a trivial undertaking. Modeling techniques, such as agent-based modeling (ABMs), take a ground-up approach by modeling the micro-scale interactions that are then observed at macro-level (population level) scales (e.g., Bhavnani, Findley, and Kuklinski 2009, Epstein 2002, Jager, Popping, and Van de Sande 2001, Kim and Hanneman 2011, Torrens and McDaniel 2013, Wijermans, Jorna, Jager, van Vliet, and Adang 2013). In this paper, we consider a model that simulates rioting in an informal settlement in Kenya that outputs the number of rioting members of a population in one minute increments (Pires and Crooks 2017). The model itself is rooted in numerous assumptions of theoretical social connections and influence of individuals. However, the emergent population level effects - the number of protesters over time - are more difficult to compare in terms of theoretical consonance.

The aim of this work is to develop methods to better understand and interpret the emergent behavior which is rooted in the value of creating ABMs. Unlike a simple representation, the ABM is what can help us better understand the underlying dynamics that lead to emergent social phenomena, such as rioting. Instead of identifying individual factors specific to events, we adopt an approach to compare the population protest behavior in the ABM. Similar in practice to measuring the characteristic length of the complex shape of an airfoil (Munson, Young, and Okiishi 2006), the observed behaviors in a social interaction are incorporated into what can be viewed as a characteristic network, a top down stylistic model of network influence. With the understanding that models of social influence are highly complex and specific networks, we seek a simple representation of the system dynamics that is able to discriminate behaviors in different event datasets. Therefore, this paper addresses the question: *Using minimal assumptions on social interactions, can our proposed characteristic model describe the temporal aspects of collective protest behavior seen in the ABM?*

The characteristic model derives from the Decision Making Model (DMM) (West, Turalska, and Grigolini 2014), an approximate model for phase transitions. In this framework, individuals are assumed to be connected, and these individuals imitate each other. Central to the first part of the assumption is that links representing influence exist between all individuals. This can potentially occur via information propagation over social media and other latent networks (e.g., Jin et al. 2014). The second part of the assumption follows from individuals tending to mimic actions and achieve influence via interactions. A theoretical treatment by Zipf makes similar arguments for seeking least effort with tools closest to one's disposal (Zipf 1949). Furthermore, other research posits that social diffusion occurs as a consequence of imitation effects specific to particular agents (Oliver and Myers 1998). The main feature of the DMM is that it uses a double-well potential function to model macro-level shifts in collective behavior. The macro-state settles into one of the two wells, but is subject to random fluctuations that can drive the state over a barrier and into the other well (e.g., phase transition). Brownian motion is used to model these fluctuations in the present model; however, other choices include fractional Brownian motion (Mandelbrot and Ness 1968) and fractional diffusion models (Baleanu et al. 2012) where history is a more prevailing factor. In this work, we adopt the completely connected double-well potential model as a basis of comparison for the duration of protest behavior in a temporal distribution, but we do not specify nodes as individual actors present in reality. Rather, we treat the nodes as abstract entities that only exist as sources of influence. From this view, the model is a parameterized generator of collective dynamics - *a unit (tuple) of comparison*.

2 AGENT-BASED MODEL OF RIOTING

The agent-based model was motivated by riots that broke-out shortly after the 2007 Kenyan presidential election results were announced. Perceptions of government illegitimacy, long-held grievances, and a history of political and economic ethnic exclusion led many to believe that election results were rigged. Two months of violence resulted in 1,100 deaths and up to 350,000 internally displaced people across Kenya (De Smedt 2009). While the violence spread across the country, Kibera, an informal settlement in Kenya's capital, became the "epicenter" of the riots in the capital (International Crisis Group 2008).

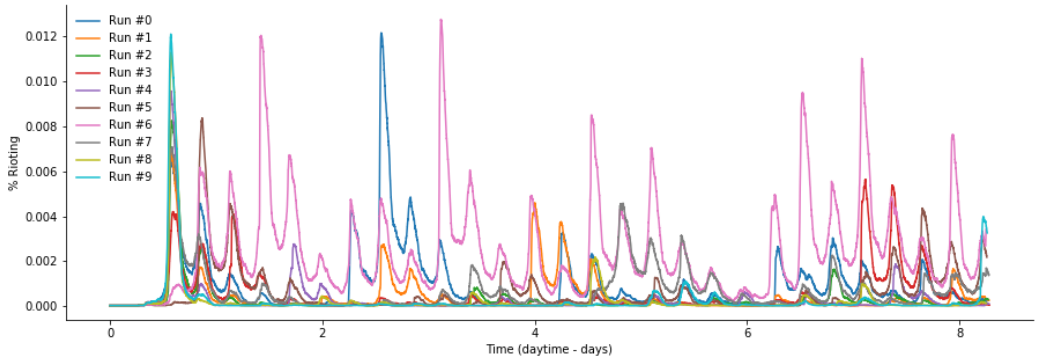

Figure 1: Timeseries output for the ABM model for ten simulations. These are the ABM data that we will fit to a characteristic model.

In order to capture the complexities associated with these riots, the ABM uses insights from the Social Sciences, the Humanities, and other disciplines focusing on the understanding of human behavior in a social-economic context (Diallo et al. 2019). It parallels the method of artificial societies, which extends the agent metaphor by grounding the rules in research of computational social science (Tolk, Pires, and Cline 2022). Socially capable agents interact within multiple social networks, from family to school and work relationships to political affiliations. They are situated in a common virtual environment that represents physical resources and constraints, but that also represents social determinants of interest.

The ABM is based on the geospatial information and activity data of the Kibera population. These interactions are captured in a cognitive model for each agent that assumes specifics regarding individual identity including social status, emotion, and physical stasis. The cognitive model then generates behavior within a parameterized environment of other individuals. The details, both theoretically and data-driven, are numerous. The environment alone consists of over 30 parameters of structures, facilities, residents, and households. The interaction strength is measured by the logistic function and distance to other individuals. The ABM is described in detail in Pires and Crooks (2017).

The degree of model fidelity gives excellent grounding for the known conditions and constraints placed on the environment. However, we are now interested in the case where we want to compare these models to known, stylistic approaches, to reduce the number of factors used to describe the model. In other words, can we describe the detail of the ABM in terms of a much simpler stylistic, but similarly complex model in terms?

To demonstrate the approach, we use 10 runs of the ABM model at the default initial conditions (Pires and Crooks 2017). The model output details the percentage of rioting members of the environment in one minute intervals spanning only daytime hours for the course of approximately one week's time. The model outputs are given in Figure 1. Each timeseries shows the ebb and flow of protests. The outcomes display coherent cyclic activity, but varying levels of protesting member of the population. This is the set of data that we use to fit the characteristic model described in the next section.

3 CHARACTERISTIC MODEL FRAMEWORK FOR PROTEST BEHAVIOR

Consider a collection of N nodes that represent influential entities, and interactions between nodes are represented by an undirected network $G(N,L)$. The set of links (edges) between nodes is denoted by L, and each edge $ij \in L$ is given a weight $w_{ij} \in \mathbb{R}^+$, which represents the local influence between two individual entities. The simplified characteristic network of the true population is assumed to be a fully connected network with

uniform edge weights where a set of principal interacting entities have network dynamics representative of those in the true population. Explicitly, the adjacency matrix $A(L)$ is everywhere nonzero except for the diagonal (i.e., $a_{ij} = w > 0, \forall ij \in L$ s.t. $j > i$).

Each node $i \in \{1,2,3,...,N\}$ is in state $s_i \in \{0,1\}$ indicating non-protest and protest activity, respectively. For a single node, the probability of protest at each time step is

$$p_p(t) = P(s_i = 1|t) \tag{1}$$
$$p_n(t) = P(s_i = 0|t) \tag{2}$$

where $p_p(t)$ is the probability that an individual entity seeks to protest at time t, and $p_n(t)$ is the probability that an entity does not seek to protest at time t. The constraint $p_p(t) + p_n(t) = 1, \forall t$ follows from the two-state system.

The likelihood of a node protesting in an isolation network (i.e., $w = 0$) is modeled as a system with maximum-entropy decay,

$$\frac{dp_p(t)}{dt} = -g[p_p(t) - p_n(t)] \tag{3}$$
$$\frac{dp_n(t)}{dt} = -g[p_n(t) - p_p(t)] \tag{4}$$

where g is the rate at which the probabilities exponentially converge to uniform protest likelihood, $p_p = p_n = 0.5$, at equilibrium. As g decreases, the required duration for the probability to reach equilibrium increases.

Dynamics at the node level induce collective behavior through influence when $w > 0$. The mean-field approximation of the probability of the population protesting (and non-protesting) is given by the number of nodes in state s at any point in time,

$$N_s = \frac{|\{i \in N : s_i = s\}|}{N} \tag{5}$$

where $||$ is the cardinality of the set of nodes in state $s \in \{0,1\}$. At the macro-level, the population protest measure is given by

$$\xi(t) = N_1 - N_0 \tag{6}$$

where $\xi(t) \mapsto [-1,1]$ measures the population propensity to protest at time t. When $\xi = 1$ ($\xi = -1$), all nodes are in a protest (non-protest) state, and $\xi = 0$ indicates that the node population is equally divided between the two states. Convergence rates, g_1 and g_0, of the fully connected network are given by

$$g_1 = \quad ge^{w[N_1 - N_0]} \quad = ge^{w\xi} \tag{7}$$
$$g_0 = \quad ge^{w[N_0 - N_1]} \quad = ge^{-w\xi} \tag{8}$$

where g is the base convergence rate defined previously. The parameter g_1 is the global influence toward protesting, $s = 1$, which depends on the relative difference of the population sizes in each state. In other words, the greater the size of the protesting population in comparison to the population not protesting, the more pressure toward protesting. Similarly, g_0 is the global influence toward not protesting, $s = 0$. Taking the time derivative of the mean-field approximation of Eq. 6 and substituting in Eqs. 8 and 7, yields the following stochastic Langevin equation

$$\frac{d\xi}{dt} = \underbrace{-g(e^{w\xi} + e^{-w\xi})\xi + g(e^{w\xi} - e^{-w\xi})}_{-\frac{dV}{d\xi}} + \varepsilon \tag{9}$$

where the term $\varepsilon \sim \mathcal{N}(0,\sigma)$ is a random time independent fluctuation with an amplitude that varies with the population count, i.e., $\sigma \propto \frac{1}{N}$. As $N \to \infty$, the fluctuations have less strength, and the effect of individual node fluctuations are dampened in a larger population.

Integrating $\frac{dV}{d\xi}$ with respect to ξ yields the potential function,

$$V(\xi) = \frac{2g}{w}\left[\xi \sinh w\xi - \frac{w+1}{w}\cosh w\xi\right] \tag{10}$$

which is representative of the effort required to shift $\xi(t)$ from one steady state of protest behavior to another. When $w \leq 1$, the potential function has one minimum at $\xi = 0$, and $\langle\xi\rangle_{t\to\infty} = 0$. A bifurcation occurs at $w = 1$ where the local influence of neighboring nodes results in collective behavior (consensus) and population level indifference becomes unstable. When $w > 1$, the potential function becomes a double-well with a local maximum at $\xi = 0$ and two minima equidistant from the origin as shown in Fig. 2. The local maximum forms a state transition barrier of height $b_{w,g} > 0$, and the expected state value approaches the minimum $\langle\xi\rangle_{t\to\infty} = \pm d_{w,g}$, where $d_{w,g} > 0$ is a distance measure from the origin. Movement between wells results from random fluctuations, ε, which have a magnitude inversely proportional to N. The collective behavior, ξ, could either be to protest or not depending on which well the trajectory settles in as shown by Fig. 2. The distribution of durations for each type of collective behavior is fully described by the parameters, N, g, and w. General properties of the double-well model can be found in West, Turalska, and Grigolinni (2014).

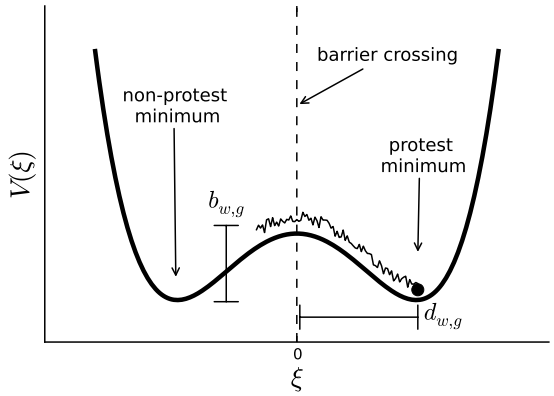

Figure 2: The potential function guides the population protest measure to one of the minima, and random fluctuations disturb this action. The probability of transferring between states depends on the strength of the fluctuations, barrier height $b_{w,g}$ and well distance $d_{w,g}$.

Given the transition dynamics in Eq. 9 and the potential in Eq. 10, the probability, $p(\xi,t)$, of the population being in ξ at time t is

$$\frac{\partial p(\xi,t)}{\partial t} = -\frac{\partial}{\partial \xi}\left[-p(\xi,t)\frac{dV(\xi,t)}{d\xi}\right] + \frac{\sigma^2}{2}\frac{\partial^2 p}{\partial \xi^2} \tag{11}$$

where $\sigma = \frac{\beta}{N}$ and $\beta > 0$ is a constant. The macro-state likelihood after a phase transition is the solution to Eq. 11 with initial condition $\xi = 0$. Integrating over the spatial domain gives the duration probability of remaining in a particular well,

$$\Gamma(t) = P(t < 0 | \xi(0) = 0) = \int_\Omega p(\xi,t)d\xi \tag{12}$$

where $\xi(0)$ is the first crossing time, $p(\xi,t)$ is the Fokker-Planck solution, Ω is the spatial domain of one well, and the initial and boundary conditions for Eq. 11 are given by

$$p(\xi,0) = \delta(0) \tag{13}$$
$$p(0,t) = 0 \tag{14}$$
$$p(\xi > c,t) = 0 \tag{15}$$

and $c > 1$ is some constant. The result is a library of candidate distributions obtained by varying the parameters g, w, N, and numerically integrating Eq. 12.

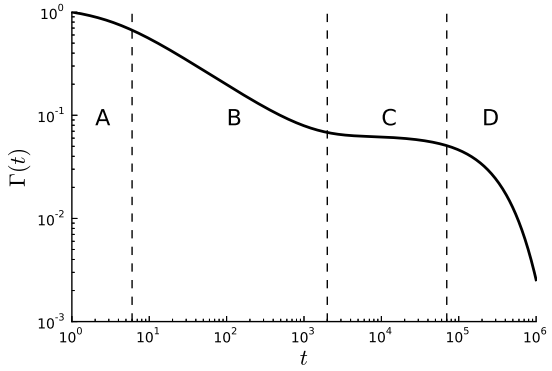

Figure 3: A diagram of a typical first crossing time distribution. Four regions separate the distribution into parts A, B, C and D. Region A occurs just after transition. The shorter this region, the more likely it is to see a repeated transition. Region B displays power law effects. Region C is Kramer's shoulder for tail effects. Region D is marked by an exponential truncation in probability.

A typical survival probability distribution produced by the model is shown in Fig. 3. It consists of four regions. Region A is marked by an initial latency before a major transition is likely to occur again. Shorter temporal spans of this region incur more of the "Joseph Effect" (Mandelbrot and Hudson 2006), or more transitions occurring after a recent occurrence. Region B has a characteristic power law decay with respect to expected duration. In terms of staying in a particular well, this region has a "Matthew Effect" (Merton 1968) due to the increasing likelihood of not switching as the duration increases. Region C is a Kramer's shoulder (Kramers 1940) marked by low probability tail events, the "Noah Effect" (Mandelbrot and Hudson 2006) or sudden changes after prolonged periods of no switching. Lastly, Region D is an exponential decay in probability that acts as a barrier to switching. At this point of prolonged duration, the macro-state will have already switched or likely never will.

3.1 Solving the Fokker-Planck Equation

Although well known, we present our approach to solving explicitly for replication. The characteristic model assumes that the evolution of the state trajectory follows

$$\frac{d\xi(t)}{dt} = -\frac{dV(\xi)}{d\xi} + \frac{1}{N}dB_t \tag{16}$$

where ε has been replaced by the Wiener differential. The Fokker-Planck solution identifies the probability, $p(\xi,t)$, that a trajectory will be in a particular state at time t, given an infinite ensemble of trajectories, $\xi(\cdot) \in \hat{\Xi}$. Given Eq. 16 and using the Komolgorov forward probability for Itō integrals results in the Fokker-

Planck equation for the macro-level protest measure

$$\frac{\partial p(\xi,t)}{\partial t} = -\frac{\partial}{\partial \xi}\left[-p(\xi,t)\frac{dV(\xi,t)}{d\xi}\right] + \frac{\sigma^2}{2}\frac{\partial^2 p}{\partial \xi^2} \tag{17}$$

where $\sigma = \sqrt{\frac{\beta}{N}}$ and $\beta > 0$ is a constant. The first partial derivative on the right side of the equation is a drift in the probability governed by the double-well potential function. The second term, $\frac{\sigma^2}{2}\frac{\partial^2 p}{\partial \xi^2}$, is the probability diffusion resulting from the random fluctuations. Solving this partial differential equation (PDE) yields the probability of the value of the protest measure at a specific time t. Absorbing boundary conditions, $p(\xi_a) = p(\xi_b) = 0$, are placed on the closed interval, $[\xi_a, \xi_b] \subset \mathbb{R}$. These conditions indicate that probability is removed when a boundary state is reached. The initial condition is prescribed as $p_0 = p(\xi, t_0)$.

Possible solution methods for Eq. 17 include finite differences or finite elements (e.g., Pichler, Masud, and Bergman 2011). The robust and simple finite difference scheme employed here uses Runge-Kutta differencing for the temporal dimension and central differences for the spatial dimension. The spatial differences used for the numerical solution are given as

$$\begin{aligned}\frac{\partial p_j}{\partial t} = \frac{d^2 V_j}{d\xi^2} p_j + \frac{dV_j}{d\xi}\frac{p_{j+1} - p_{j-1}}{2\Delta\xi} \\ + \frac{\sigma^2}{2}\frac{p_{j+1} + p_{j-1} - 2p_j}{\Delta\xi^2} + \mathscr{O}(\Delta\xi^2)\end{aligned} \tag{18}$$

where $j \in \{1, 2, \ldots, J\}$ is a uniform spatial lattice index with increments $\Delta\xi$. The notation in the above equation is shortened so that $p_j = p(\xi_j, t)$, $V_j = V(\xi_j, t)$. Solving over a discrete lattice using Eq. 18 requires the initial condition in Eq. 13 to be relaxed to

$$p(\xi, 0) = \mathscr{N}(0, \alpha) \tag{19}$$

where the parameter $\alpha \gg \Delta\xi$ must be sufficiently large to ensure a good numerical approximation. Eq. 18 is solved using the Scipy (Virtanen, Gommers, Oliphant, et al. 2020) package real-valued variable-coefficient ordinary differential equation solver ("vode") and backward differentiation formulas ("bdf"). A solver order of 15 is adequate for maintaining solver stability with parameter combinations resulting in stiff systems. Conditions where stiffness becomes a problem occur when the probability flow becomes trapped in a steep well with small escape probability.

3.2 Sampling Methods

We determine the empirical survival probability distribution (SPD) from the ABM, $\hat{\Gamma}(t)$, using the protest time series shown in Figure 1. We perform the analysis using an hour time resolution. The hourly time series of the number of protest events from the ABM is represented by

$$e_k \mapsto \mathbb{Z}^+, k \in \{0, 1, \ldots, K\} \tag{20}$$

where $k = 0$ corresponds to the first hour and $k = K$ corresponds to the last hour in the data. Protest states occur when

$$\hat{x}(k) = \mathbb{1}(e_k > \alpha) \tag{21}$$

where $\mathbb{1}(\cdot)$ is the indicator function and α is a threshold for protests. Therefore, $\xi(t) > 0$ when $\hat{x}(k) = 1$, and $\xi(t) < 0$ when $\hat{x}(k) = 0$.

The choice of α is purely definition and directly effects the protest sampling. Essentially, the α threshold defines when the population is in the macro-level protest state and when it is not. This is a tough decision, in general, because a protest is hard to define a priori and difficult to assign to a number. In other words, one knows a protest only after it occurs. Therefore, we adopt the approach of scaling the protest threshold value in 0.001% population increments over the range $[0.001, 0.01]$. We will see in the results section how the fit to the characteristic model changes with the choice of threshold.

The difference of $\hat{x}(k)$ estimates the barrier crossings when $\xi = 0$, as depicted in Fig. 4. The transition indicator function is given by

$$\hat{\delta}\xi(k) = \mathbb{1}\left(\hat{x}(k+1) - \hat{x}(k)\right) \tag{22}$$

which indicates that at time interval, k, the macro-state experienced a transition. The sequence,

$$k_j^* = \{k, \hat{\delta}\xi(k) = 1\}, j \in \{0, 1, \ldots, J\} \tag{23}$$

identifies transitions for all temporal durations of a particular time series containing J transitions. The time duration for a given transition is

$$\hat{\delta}t(j) = k_{j+1}^* - k_j^* \tag{24}$$

for a particular transition time, k_j^*. Here, $\hat{\delta}t(j)$ is a random variable. The measured SPD, $\hat{\Gamma}(t)$, is the complementary cumulative probability function

$$\hat{\Gamma}(t) = P(\tau > t | \xi(\tau) = 0, \xi(t_0) = 0, t_0 < t). \tag{25}$$

To produce the SPD, the normalized probability distribution function is given by the Kaplan-Meier estimator,

$$\hat{\Gamma}(t) = \prod_{\omega < t} \left[1 - \frac{\sum_{j=0}^{J} \mathbb{1}_{\omega}(\hat{\delta}t(j))}{J - \sum_{j=0}^{J} \mathbb{1}_{<\omega}(\hat{\delta}t(j))} \right], \omega \in \mathbb{N} \tag{26}$$

In practice, the first data point (first product), will not be known due to resolution constraints which affects the overall normalization of the empirical distribution. Therefore, we normalized the SPD to match the area under the curve of the candidate theoretical distributions.

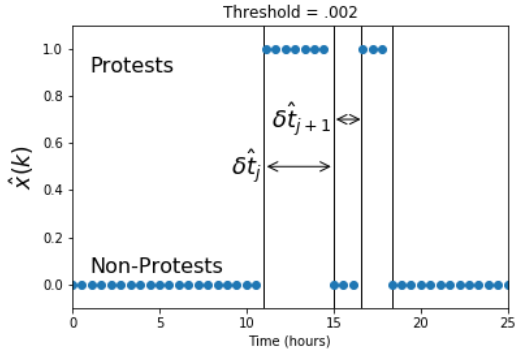

Figure 4: Sampling methodology. This example protest time series signal, $\hat{x}(k)$, is used to identify transition durations, $\delta\hat{t}$, for each run of the ABM. A value of 1 indicates a protest occurred on that date.

4 ANALYSIS & RESULTS

The protest duration results of the ABM riot model and the theoretical results of the characteristic model are compared using point-wise distance errors at each point of the measured distribution. Example fits are

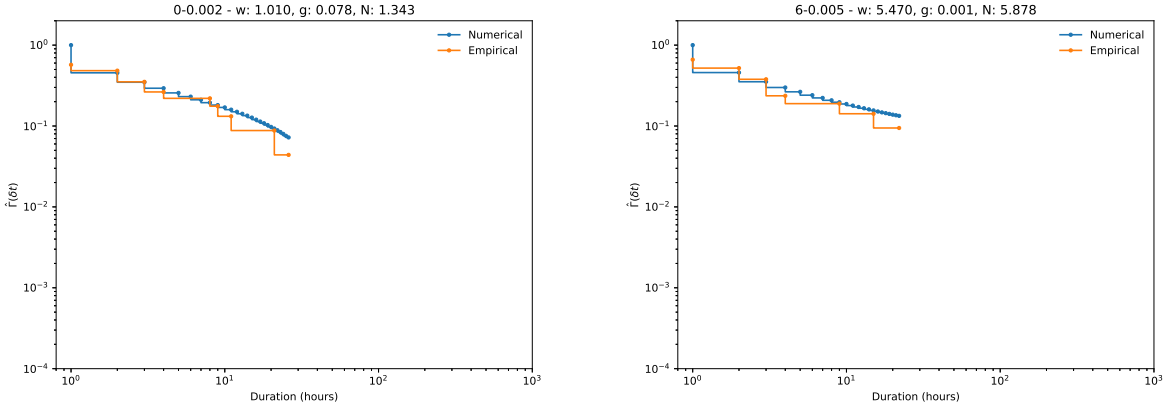

(a) Run 0 - .002 Threshold

(b) Run 6 - .005 Threshold

Figure 5: Distribution matching from the ABM to the Characteristic Model. Two examples of fitting are shown. Examples chosen to show difference in distribution type. The former is more characteristic of individual network coherence; the latter displays more group dynamics and well activity. Both have relatively low time constants.

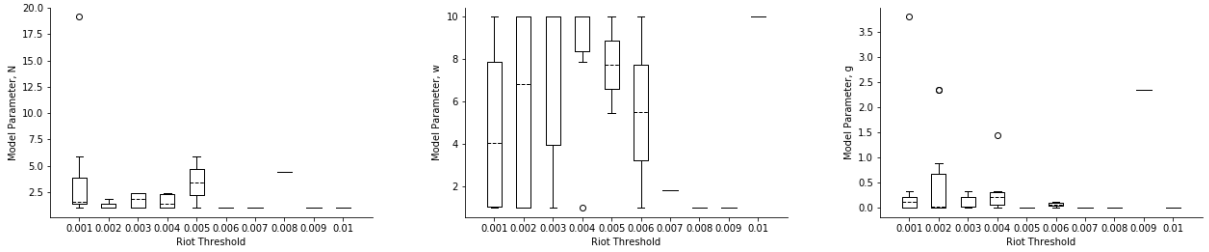

(a) Population Parameter, N

(b) Well Height Parameter, w

(c) Time Constant Parameter, g

Figure 6: Parameter distributions realized from each of the ABM iterations.

displayed in Figure 5. The method of comparison was to choose a set of parameters for the theoretical distribution and use a nearest neighbor approach to select the parameters.

Fits were performed for every threshold of the ABM riot model in the range $[.001, .01]$ in .001% increments. As the the thresholds increased to $> .005\%$ rioting population, we found that there were many protest durations that did not have a nearest neighbor to a characteristic model. This is because the survival probability distribution was concentrated on either 0 or indefinite durations - outside of the parameter sweep performed by the characteristic model. These extremes are removed, because they are not ordinarily captured by this type of characteristic model and don't provide much useful durational information. The parameters g, w, and N are displayed in Figure 6.

From the resolved parameters, we can make a number of different observations about the duration dynamics of the protest model. First, the parameters tend to favor the lower ends of the spectrum for both the population number and time constant. This indicates that relative to the characteristic model, the individual interactions leading to the population states occur relatively slowly compared to the fully connected model. The population parameter is quite small as well, indicating that the macro-state tends to exhibit behavior

associated with a single decision maker versus a group. However, in the lower threshold region, we see more variation and increases in these two parameters. This is likely a result of the very low threshold for macro-state changes.

Second, we see that the well height parameter varies comparatively more over all riot thresholds. The well height parameter is a direct adjustment on the relative difficulty for crossing from one well to the other. In comparison to the characteristic model, the ABM is displaying more variation with each run with respect to this parameter. This is an important distinction because it shows that the initial conditions of the model and the interactions therein can result in different population outcomes displaying more or less difficulty for population level transitions.

Overall, the parameters corresponding to the characteristic model are of descriptive value. The many parameters of the agent-based model are condensed into three parameters that directly correspond to the population-level transition probability from protest to non-protest states. With this, similarities and differences among the agent-based model results are reflected. However, it remains to show whether there is any predictive value in the technique, such as that seen in methods of factor analysis.

5 CONCLUSION AND FUTURE RESEARCH

In this paper, we discuss a method whereby simulation outcomes produced by an agent-based modeling approach to studying rioting within a population is parameterized by a simpler characteristic and stylistic reference model. The purpose for undergoing this exercise is to reduce the burden of description of a given model to fewer parameters to enable comparisons to dynamics of interest. Presently, we have described the process and demonstrated how this can be done for the case of protest duration. Additionally, we show how the realized parameters can vary not only with the model instantiations, but with the exogenous requirements imposed at application time.

One major question that remains is one regarding the use of the characteristic model to make predictions regarding complex outcomes. Although useful from a descriptive point of view, the additional step that needs to be taken is to explore the ability of the parameters to serve as useful predictors and the amount of information needed to generate the predictors. Similar to methods of factor analysis, useful predictors based on a characteristic model can be used to greatly simplify subsequent actions or forecasts made.

Another area of future evaluation involves enhancing the ABM. One focus would be incorporating what can be learned from other simulations with similar measures determined by the characteristic model. This technique could also find possible use in policy evaluation by further capturing methods of the artificial societies. This would allow us to gain additional insights into the complexity of the modeling and simulation challenge to better trace the impact of policies impacting and affected by protest occurrences.

ACKNOWLEDGMENTS AND DISCLAIMER

The authors would like to thank Heather Rosso and Andreas Tolk for their review and feedback of the paper.

The author's affiliation with The MITRE Corporation is provided for identification purposes only, and is not intended to convey or imply MITRE's concurrence with, or support for, the positions, opinions, or viewpoints expressed by the author.

REFERENCES

Baleanu, D. et al. 2012. *Fractional Calculus: Models and Numerical Methods*, Volume 3 of *Series on Complexity, Nonlinearity and Chaos*. New Jersey, World Scientific.

Bhavnani, R., M. G. Findley, and J. H. Kuklinski. 2009. "Rumor dynamics in ethnic violence". *The Journal of Politics* vol. 71 (3), pp. 876–892.

Braha, D. 2012. "Global Civil Unrest: Contagion, Self-Organization, and Prediction". *PLoS ONE* vol. 7 (10), pp. e48596.

Casper, B. A., and S. A. Tyson. 2014. "Popular Protest and Elite Coordination in a Coup d'état". *The Journal of Politics* vol. 76 (2), pp. 548–564.

Clauset, A., M. Young, and K. S. Gleditsch. 2007. "On the Frequency of Severe Terrorist Events". *Journal of Conflict Resolution* vol. 51 (1), pp. 58–87.

De Smedt, J. 2009. "'No Raila, No Peace!' Big man politics and election violence at the Kibera grassroots". *African Affairs* vol. 108 (433), pp. 581–598.

Diallo, S. Y. et al. (Eds.) 2019. *Human simulation: perspectives, insights, and applications*. Cham, Switzerland, Springer Nature.

Epstein, J. M. 2002. "Modeling civil violence: An agent-based computational approach". *Proceedings of the National Academy of Sciences* vol. 99 (suppl 3), pp. 7243–7250.

Fowler, J. H., and N. A. Christakis. 2010. "Cooperative behavior cascades in human social networks". *Proceedings of the National Academy of Sciences* vol. 107 (12), pp. 5334–5338.

González-Bailón, S. et al. 2011. "The Dynamics of Protest Recruitment through an Online Network". *Scientific Reports* vol. 1 (197).

International Crisis Group 2008. "Kenya in crisis".

Jager, W., R. Popping, and H. Van de Sande. 2001. "Clustering and fighting in two-party crowds: Simulating the approach-avoidance conflict". *Journal of Artificial Societies and Social Simulation* vol. 4 (3), pp. 1–18.

Jin, F. et al. 2014. "Modeling Mass Protest Adoption in Social Network Communities Using Geometric Brownian Motion". In *Proceedings of the 20th ACM SIGKDD International Conference on Knowledge Discovery and Data Mining*, KDD '14, pp. 1660–1669. New York, NY, USA, ACM.

Johnson, N. F. et al. 2013. "Simple Mathematical Law Benchmarks Human Confrontations". *Scientifc Reports* vol. 3 (3463).

Kim, J.-W., and R. Hanneman. 2011. "A computational model of worker protest". *Journal of Artificial Societies and Social Simulation* vol. 14 (3), pp. 1.

Kramers, H. 1940. "Brownian motion in a field of force and the diffusion model of chemical reactions". *Physica* vol. 7 (4), pp. 284 – 304.

Lorenz, E. N. 1963. "Deterministic nonperiodic flow". *Journal of the atmospheric sciences* vol. 20 (2), pp. 130–141.

Mandelbrot, B., and R. L. Hudson. 2006. *The Misbehavior of Markets: A Fractal View of Financial Turbulence*. New York, Basic Books.

Mandelbrot, B. B., and J. W. V. Ness. 1968. "Fractional Brownian Motions, Fractional Noises and Applications". *SIAM Rev.* vol. 10 (4), pp. 422–437.

Merton, R. K. 1968. "The Matthew Effect in Science". *Science* vol. 159 (3810).

Munson, B. R., D. F. Young, and T. H. Okiishi. 2006. *Fundamentals of Fluid Mechanics*. 5 ed. Hoboken, NJ, Wiley.

Nicolelis, M. 2012. *Beyond Boundaries: The New Neuroscience of Connecting Brains with Machines—and How It Will Change Our Lives*. New York, St. Martin's Griffin.

Oliver, P. E., and D. J. Myers. 1998. "Diffusion models of cycles of protest as a theory of social movements". *Presented at the Congress of the International Sociological Association*.

Pichler, L., A. Masud, and L. Bergman. 2011. "Numerical Solution of the Fokker-Planck Equation By Finite Difference and Finite Element Methods - A Comparative Study". In *3rd ECCOMAS Thematic Conference on Computational Methods in Structural Dynamics and Earthquake Engineering*, COMPDYN 2011.

Pires, B., and A. T. Crooks. 2017. "Modeling the emergence of riots: A geosimulation approach". *Computers, Environment and Urban Systems* vol. 61, pp. 66 – 80.

Tolk, A., B. S. Pires, and J. C. Cline. 2022. "Artificial Societies Enabling Multidisciplinary Policy Evaluation – A Health Policy Example". In *Proceedings of MODSIM World 2022, in press*.

Torrens, P. M., and A. W. McDaniel. 2013. "Modeling geographic behavior in riotous crowds". *Annals of the Association of American Geographers* vol. 103 (1), pp. 20–46.

Virtanen, P., R. Gommers, T. E. Oliphant et al. 2020. "SciPy 1.0: Fundamental Algorithms for Scientific Computing in Python". *Nature Methods* vol. 17, pp. 261–272.

West, B. J., and P. Grigolini. 2011. *Complex Webs*. Cambridge, Cambridge University Press.

West, B. J., M. Turalska, and P. Grigolini. 2014. *Networks of Echoes: Imitation, Innovation, and Invisible Leaders*. Switzerland, Springer International Publishing.

Wijermans, N., R. Jorna, W. Jager, T. van Vliet, and O. Adang. 2013. "Cross: modelling crowd behaviour with social-cognitive agents". *Journal of Artificial Societies and Social Simulation* vol. 16 (4), pp. 1.

Zipf, G. K. 1949. *Human Behavior and the Principle of Least Effort*. Cambridge, Addison-Wesley Press, Inc.

AUTHOR BIOGRAPHIES

BRIAN J. GOODE is a Lead Gaming & Simulation Engineer at The MITRE Corporation. Dr. Goode holds a Ph.D. in mechanical engineering from Virginia Tech. His email address is bgoode@mitre.org.

BIANICA PIRES is a Lead Modeling & Simulation Engineer at The MITRE Corporation. Dr. Pires holds a Ph.D. in computational social science from George Mason University. Her email address is bpires@mitre.org.